Role of the grain size on the hydration characteristics of slag in an aged field concrete

Zhang, Yu; Çopuroğlu, Oğuzhan

DOI
10.1016/j.cemconres.2022.106985

Publication date
2022

Document Version
Final published version

Published in
Cement and Concrete Research

Cement and Concrete Research 162 (2022) 106985

Contents lists available at ScienceDirect

Cement and Concrete Research

journal homepage: www.elsevier.com/locate/cemconres

Role of the grain size on the hydration characteristics of slag in an aged field concrete

Yu Zhang *, Oğuzhan Çopuroğlu

Microlab, Section of Materials and Environment, Faculty of Civil Engineering and Geosciences, Delft University of Technology, Delft, the Netherlands

ARTICLE INFO

Keywords:
40-year-old slag cement concrete sample
Elemental composition
Slag size
Slag rim
Hydration mechanism

ABSTRACT

This paper studies chemical composition of partially and fully hydrated slag grains in a (nearly) 40-year-old field concrete from the Netherlands. The concrete samples were assumed to be sufficiently aged to contain fully hydrated slag grains as well as partially hydrated large slag particles with thick rims. Our analysis showed that three different elemental zoning could be identified depending on the original slag grain size. Upon full hydration of a small slag grain (i.e., <8 μm), two distinct regions were identified corresponding to a hydrotalcite-like phase in the outer rim and a C–S–H gel phase in the core, respectively. As for medium (8–17 μm) and large (>15 μm) slag grains, three distinct regions were clearly visible. Hydrotalcite-like phase was mainly observed in the outer rim and the core. C–S–H gel phase was found to be precipitated in the region between the outer rim and the core.

1. Introduction

As a mature addition in cement industry, blast furnace slag (henceforth slag) is a tried and tested, high-performance alternative that has been used for nearly a century in Europe and North America, as a supplementary cementitious material (SCM) [1–4]. The current European cement standard EN 197-1 classifies 27 different cement types, 9 of which contain slag as the main component in proportions from 6 to 95 wt%.

During the hydration of slag cement paste, the main components of cement clinker, i.e., C_3S, C_2S, C_3A, and C_4AF react at different rates to produce calcium silicate hydrate (C–S–H), portlandite, ettringite, monosulfoaluminate, hydrogarnet and other trace hydration products. On the other hand, the hydration of slag grains mainly depends on the breakdown of slag network structure by OH^- ion, in the form of alkali (Na and K) hydroxide and $Ca(OH)_2$. Slag reacts relatively slowly and can be treated as inert filler during the early stages of hydration. Secondary formations, e.g., C–S(A)–H and hydrotalcite-like phases originated from the dissolution of slag have been identified [5]. Compared with pure cement paste, blending cement with slag increases the amount of C–S(A)–H and lowers its Ca/Si atomic ratio as slag contains more SiO_2 and less CaO [6–10]. Low Ca/Si C–S(A)–H fills up the capillary pores, reduces the total porosity and thus contributes to an enhanced durability [11–13]. Moreover, hydrotalcite-like phase, considered as a functional compound with a Layered Double Hydroxides (LDHs) structure [14], is closely mixed with C–S(A)–H gel phase forming the so-called 'inner' hydration product of slag. The Mg/Al atomic ratio of this phase formed in slag cement or alkali-activated slag paste is not fixed and differs over a wide range [9,15,16]. It was observed to be close to hydrotalcite ($Mg_6Al_2(OH)_{16}(CO_3)\cdot 4H_2O$) compositionally and structurally. However, the latest findings from evolved gas studies showed that the hydrotalcite-like phase in slag cement paste was closer to meixnerite ($Mg_6Al_2(OH)_{16}(OH)_2\cdot 4H_2O$) [17].

Often, laboratory studies to investigate the hydration characteristics of slag in cementitious systems are restricted within a period of up to several years, at most. Within several years of curing, typical cement clinkers may reach a degree of hydration close to 100 %, however most of the (larger) slag grains are far from reaching their full potential with respect to their hydration degree. Therefore, many partially hydrated slag grains are visible even in a cement paste microstructure of several decades old. It is commonly postulated that slag dissolution becomes increasingly difficult at later ages. This is mainly because the hydrates being precipitated around an unreacted slag grain gradually hinder the diffusion of dissolved Ca, Si, Al and Mg from inside to outside and OH^- ion to diffuse from outside to inside. Thus, the ultimate distribution of 'inner' products after the full hydration of slag grain still tends to be a question unsolved. Moreover, only a few studies could elaborate the elemental composition of slag rim, which is a challenging work,

* Corresponding author.
E-mail addresses: Y.Zhang-28@tudelft.nl (Y. Zhang), O.Copuroglu@tudelft.nl (O. Çopuroğlu).

https://doi.org/10.1016/j.cemconres.2022.106985
Received 21 March 2022; Received in revised form 22 August 2022; Accepted 12 September 2022
Available online 18 September 2022

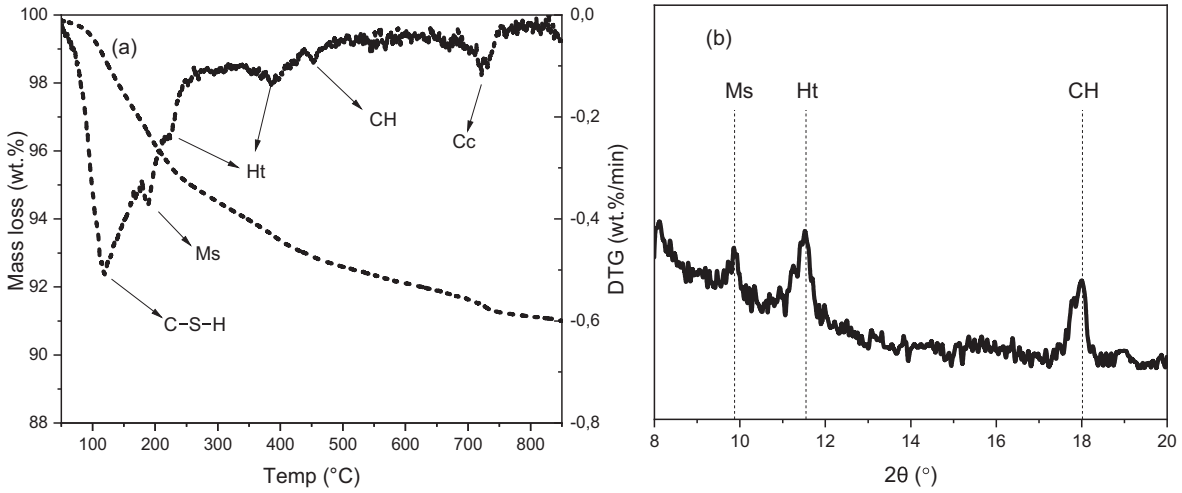

Fig. 1. (a) TG and DTG and (b) XRD results of the 40-year-old slag cement concrete. Ms: calcium monosulfoaluminate; Ht: hydrotalcite-like phase; CH: portlandite; Cc: calcium carbonate.

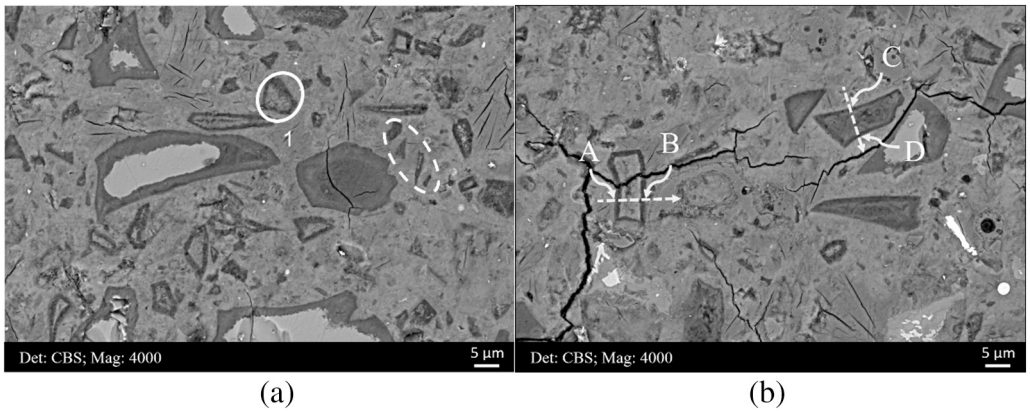

Fig. 2. Two representative BSE micrographs of the microstructure.

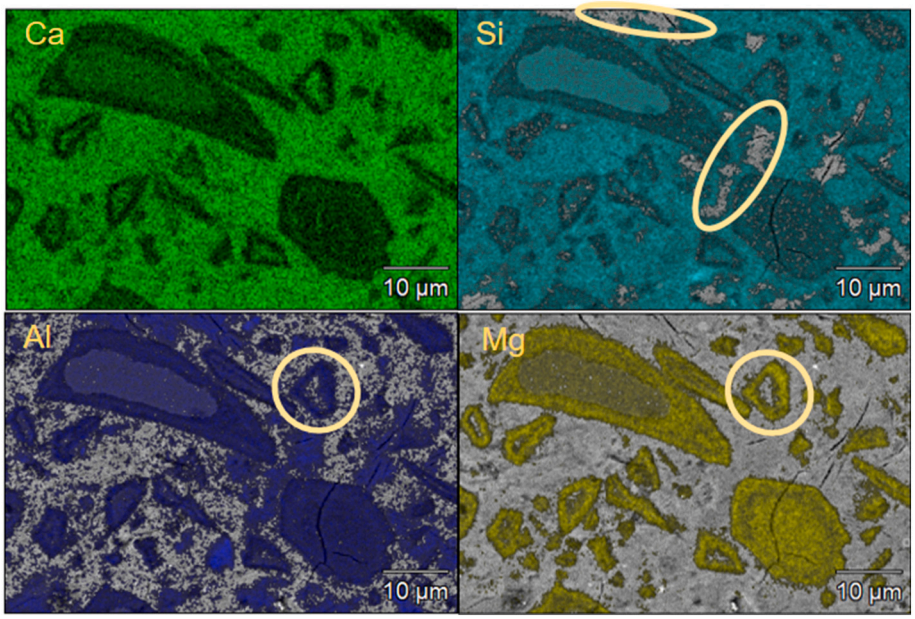

Fig. 3. Main EDS element mappings acquired from the same field of view in Fig. 2(a) in a different orientation.

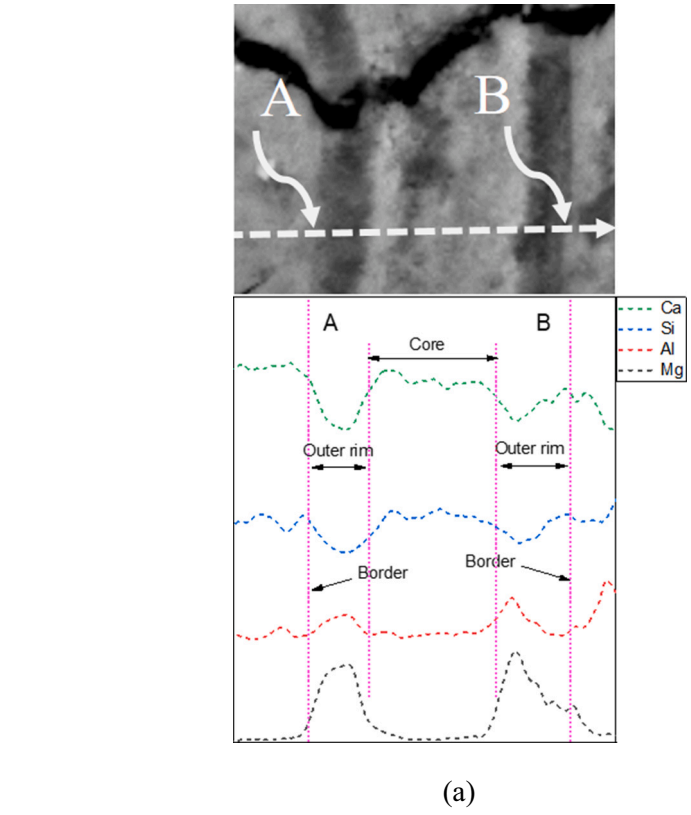

Fig. 4. (a) Linescan-profiles of Ca, Si, Al and Mg along the dissection line A-B (The distance from A to B is ~5 μm.) shown in Fig. 2(b); (b) Mg/Al and Ca/Si atomic ratios and (c) grey level values correspondingly.

particularly because it is too thin to acquire an accurate composition from a typical short-term laboratory cured sample. The work in [18] discussed the nano-structural evolution of slag rim in a slag cement paste up to 180 days and confirmed the formation of three distinct layered hydration product regions around the unhydrated slag grains due to the spatial zonation of hydrotalcite-like phase, C–S(A)–H gel phase and Ca–Al LDHs phase, respectively. The results from [19] also highlighted that the rim around a partially hydrated slag particle was a composite phase of C–S(A)–H gel phase and hydrotalcite-like phase formed by the in-situ reaction between the outer layer of slag and OH^- ions in the pore solution. The observations in [20] supported the hypothesis that the positively charged Mg-Al LDH layers were strongly attracted to the negatively charged C–S(A)–H layers in slag rim during alkali-activation by means of multiple advanced characterization techniques, e.g., FTEM and FESEM.

As in the Netherlands the history of slag cement use dates back to early 1900s, obtaining an aged slag cement concrete for the purpose of studying fully hydrated slag grains was possible. To this end, 40-year-old

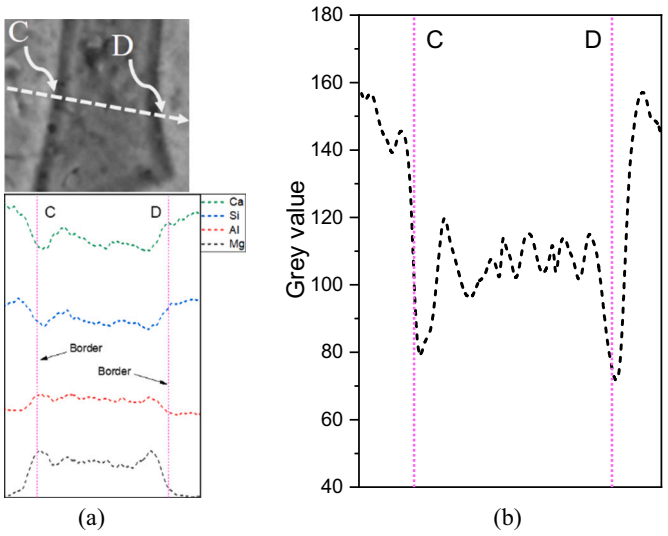

Fig. 5. (a) Linescan-profiles of Ca, Si, Al and Mg along the dissection line C-D (the distance from C to D is ~5 μm) shown in Fig. 2(b); (b) grey level correspondingly.

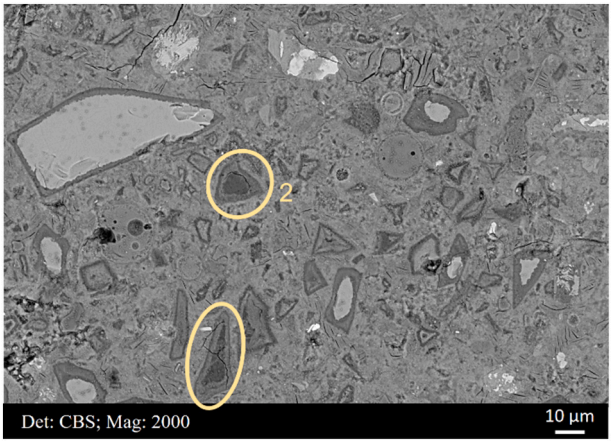

Fig. 6. Representative BSE micrograph of the microstructure.

slag cement concrete samples were collected from the field. The age of this concrete was assumed to be sufficient to allow most slag grains to have reached their hydration potential and formed thick rims around the larger slag particles. The results found in this paper provide insight into the migration of cations (Mg^{2+} ion in particular) during slag dissolution, and help understand the hydration mechanism of a single slag particle depending on its size, especially at later ages.

2. Materials and methodology

2.1. Sample information

The concrete samples were collected from Rozenburg Wind Wall (exposed to the atmosphere without contacting water) located between Road Isarweg and Neckarweg, Europoort Rotterdam (Port of Rotterdam) in the Netherlands, which was built in 1985 and produced using CEM III/B.

In order to identify the hydrates formed in the samples, thermogravimetric analysis (TGA) and X-ray diffraction (XRD) measurement were performed. Hydration of the samples was stopped by solvent exchange with isopropanol. Slices cut and selected from the samples were ground and sieved below 63 μm. TGA was performed on Netzsch STA 449 F3 Jupiter under Argon atmosphere. About 40 mg of sample powder was heated from 40 to 900 °C with a heating rate of 10 °C/min in an Al_2O_3 crucible together with an identical empty crucible as reference. XRD data was collected using a Philips PW 1830/40 Powder diffractometer with Cu K-alpha radiation. The machine was operated with an X-ray beam current of 40 mA and an acceleration voltage of 40 kV. Sample powders were scanned from 5 to 60° (2θ) with a step size of 0.03°. TG and DTG results in Fig. 1(a) shows that the small peak between 400 and 500 °C sourcing from the dehydration of portlandite almost disappears. The peaks located at approximately 250 and 350 °C indicate the presence of hydrotalcite-like phase. The mass loss at 100–150 °C suggests the presence of C–S–H gel phase. The shoulder at ~200 °C implies the formation of calcium monosulfoaluminate, originated from the transformation of ettringite with time. It is visible clearly in the samples after about 40 years. Similarly, the results of XRD confirmed the existence of monosulfate, hydrotalcite-like phase, and portlandite in the paste.

2.2. Experimental method

Samples were immersed in isopropanol solution for one week to stop hydration, dried at 40 °C oven for 1 h, and impregnated with low viscosity epoxy resin. Polished section was prepared for the microstructural analysis. The sample surface was ground with #180, #220, #320, #800, and #1200 SiC grinding papers cooled with pure ethanol sequentially, and polished by 9, 3, 1, and 0.25 μm diamond paste, in turn. After each step, the sample was immersed in an ultrasonic bath filled with 100 % ethanol for 30 s for cleaning. Finally, the well-polished sample surface was carbon coated in a Leica EM CED030 carbon evaporator at a thickness of about 10 nm.

Elemental composition of the hydrates formed during the hydration of slag grains were characterized by a FEI QUANTA FEG 650 ESEM equipped with X-ray energy dispersive detector in high vacuum chamber condition using internal microanalytical standards. The accelerating voltage and working distance used throughout the analysis were kept at 10 kV and 10 mm, respectively.

3. Results

In the present paper, we classified the slag grains into three groups based on their apparent original diameter (or size) as acquired by the BSE imaging, assuming that the slag grains retained their shape during hydration. The slag size groups were named as: small (1 μm < d < 8 μm), medium (8–17 μm), and large (>15 μm), which were hypothetically linked to different elemental zonings. For the detailed classification process, please refer to Appendix. The results are presented for each size class.

3.1. Small slag grains

3.1.1. Microstructure

Fig. 2 illustrates a homogeneous and dense matrix containing unhydrated slag particles even after around 40 years. The hydrates precipitated as rims around unreacted slag grains were observed which were integrated with the surrounding cement matrix. Additionally, fully hydrated tiny slag grains (<1 μm), as shown in dashed circles in Fig. 2 (a), were found to be dispersed throughout the microstructure. The tiny slag grains were excluded in this study due to the insufficient spatial resolution the microanalytical technique offers. Nonetheless, it is plausible to suggest that the observations on the small slag grains would provide insight for understanding the hydration characteristics of the tiny slag grains, as well.

As seen in circle 1, the outer rim of the fully hydrated small slag grain shows relatively dark coloration (representing low mean atomic number). Conversely, the core or center displays a less dark grey pixel value, almost the same coloration compared to the cement matrix. Also, it is found that the outer rim develops uniformly, and the thickness of them

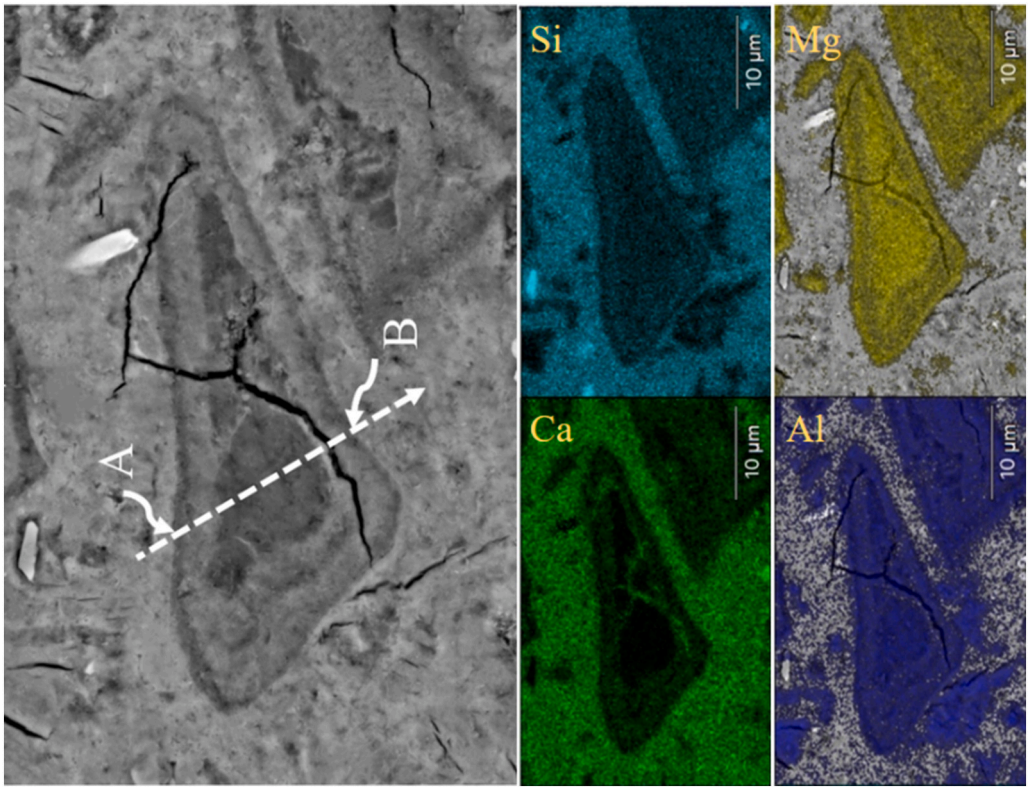

Fig. 7. A representative region in Fig. 6 presented by BSE micrograph with higher magnification and its main element mappings correspondingly. Left: BSE micrograph; Middle top and bottom: Si and Ca mappings; Right top and bottom: Mg and Al mappings.

fluctuates around 1 μm.

3.1.2. *Elemental composition*

Fig. 3 shows the EDS mappings of the main elements (Ca, Si, Al, and Mg) of Fig. 2(a). The intensity of each color is related to the concentration of the corresponding element. Higher pixel values are represented brighter, indicating higher concentrations of a given element. Magnesium appeared to be exclusively entrapped within the original slag grain boundaries. Interestingly magnesium deficiency was observed in the core region of small slag grains upon full hydration. Moreover, similar features were observed for aluminum in several other grains.

In Fig. 4(a) EDS linescan-profiles of the main elements (Ca, Si, Al, and Mg) can be seen along the dissection line A-B from Fig. 2(b). Mg/Al and Ca/Si atomic ratios, and grey level along the line are shown in Fig. 4 (b) and (c), correspondingly. Consistent with the element mappings shown in Fig. 3, aluminum and magnesium species were accumulated in the outer rim near the border, while the core was rich in calcium and silicon, deficient in aluminum, and without any trace of magnesium. The Mg/Al atomic ratio in the outer rim was about 2.0, and it drastically levelled off to null in the core. The Ca/Si atomic ratio fluctuated considerably without showing a systematic trend. Based on these results, it can be postulated that as the hydration proceeds in a small slag grain, the newly released Mg^{2+} ions tend to migrate towards the perimeter of the slag grain; however, they cannot move far away from the grain due to their low mobility and instantaneous precipitation in the form of hydrotalcite-like phase [6,7,9]. In other words, Mg^{2+} ions are captured and fixed within the outer rim. Furthermore, Al ions, which present fair mobility, move out during the hydration as confirmed in Fig. 3. At the same time, it was estimated that nearly half of the Al ions enter into the matrix and are incorporated into C–S(A)–H gel phase. (The Mg/Al atomic ratio of raw slag was just a little <1 [21] and all magnesium is fixed into hydrotalcite-like phase with a Mg/Al ratio ≈ 2.0.) Meanwhile, there were still large quantities of calcium and silicon entrapped inside the core, playing a role in the formation of C–S–H gel phase (Fig. 4(a) and (b)).

Accumulation of Al and Mg at the outer rim is further seen on BSE grey level values as shown in Fig. 4(c). Relatively lower mean atomic numbers of these elements are represented by darker grey pixels with an arbitrary value of 60 as opposed to the pixel values of the grain core. The core being rich in Ca and Si was observed lighter in color (pixel value 140) due to the higher mean atomic number in this zone. It was also noted that the core displayed a similar grey level to the surrounding matrix, indicating an almost identical mean atomic number, i.e., Ca/Si atomic ratio in principle, was formed by hydrates in the matrix and core of small slag grains.

Fig. 5(a) and (b) shows EDS linescan profiles of the elements (Ca, Si, Al, and Mg) as well as the BSE grey level values along the dissection line C-D from Fig. 2(b), respectively. On this dissection line, the grey values corresponding to the outer rim and core did not have sufficient contrast to allow visual distinction compared to the A-B dissection line. The grey value is about 80 near the outer rim and it only increases to 110 on average at the core. A tiny increase in Mg concentration, while a decrease in Ca and Si concentrations is found near the border. The trend reverses in the core, where the concentration of Mg goes down a little bit, while Ca and Si concentrations go up slightly. Neither exhaust of Mg and/or Al in the core nor apparent accumulation of them in the outer rim is observed in this case.

In fact, elemental profiles along the dissection line C-D were quite similar to the observations on the rim of slag grain shown inside Circle 3-1 in the following Section 3.3.1. Thus, it is reasonable to assume that this region does not source from a totally hydrated slag particle, rather than is cut from a thick rim along partially hydrated slag particle.

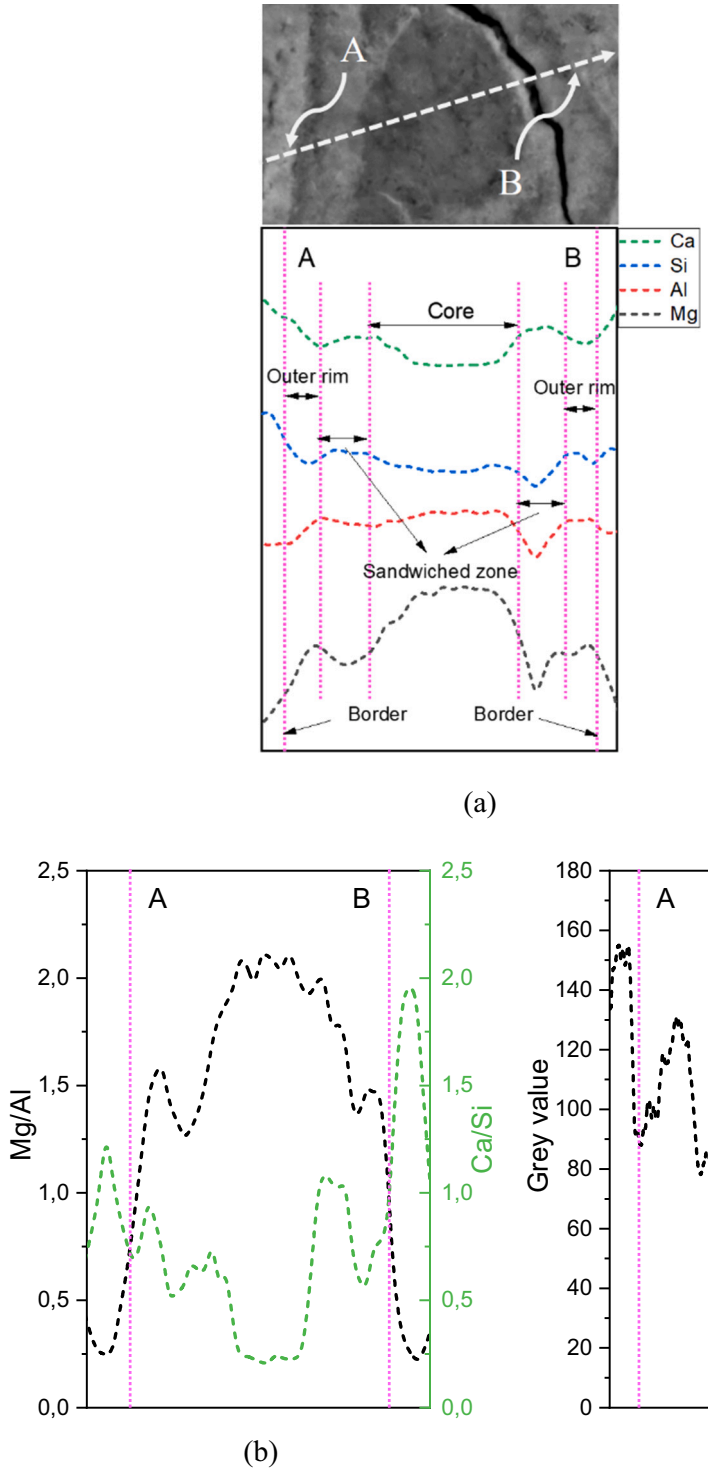

Fig. 8. (a) Linescan-profiles of Ca, Si, Al and Mg along the dissection line A-B (the distance from A to B is ~10 μm) shown in Fig. 7; (b) Mg/Al and Ca/Si atomic ratios and (c) grey level correspondingly.

3.2. Medium slag grains

3.2.1. Microstructure

In concrete with a long service life, fully hydrated slag grains of medium size (8–17 μm) are also frequently observed, two of which are encircled in Fig. 6. The elemental distribution was recognized zoning in the BSE micrograph as two distinct grey pixel values forming three zones within the medium slag grains. The outer rim area as well as the grain core show lower average atomic number while the zone in-between (named as sandwiched zone henceforth) was composed of a higher average atomic number.

3.2.2. Elemental composition

Fig. 7 displays a close-up BSE micrograph of a single medium-sized slag grain in Fig. 6, as well as its main element (Ca, Si, Al, and Mg) mappings of the same field of view. Magnesium appears to be distributed within the boundaries of the original slag grain and could not diffuse into the cement matrix. Unlike the observations on the small slag grains

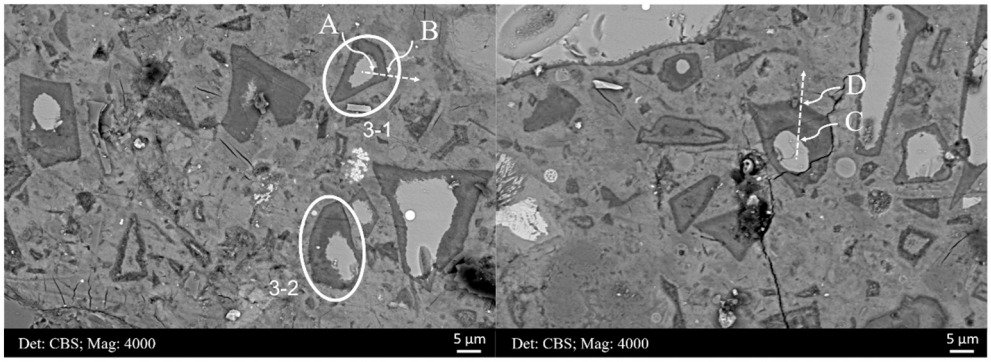

Fig. 9. Two representative BSE micrographs of the microstructure.

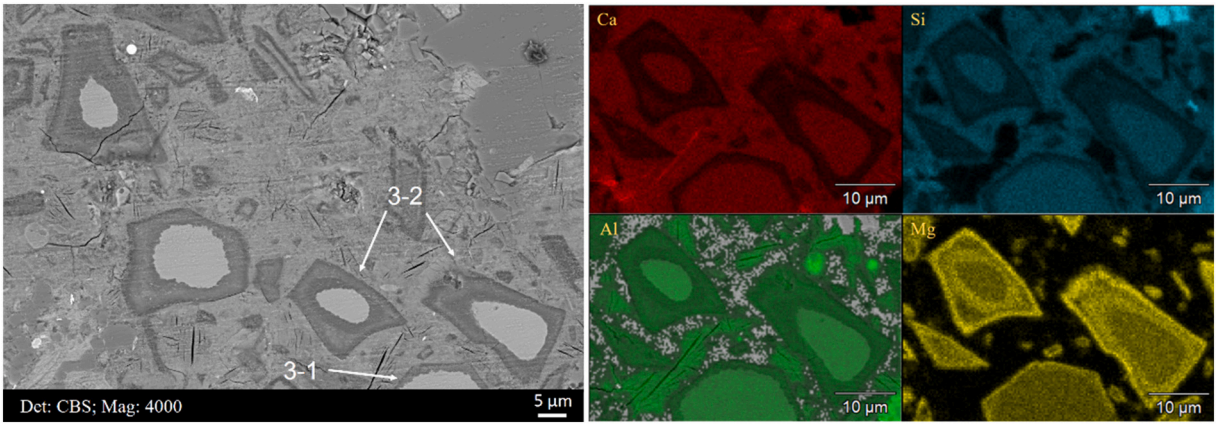

Fig. 10. A representative region and its main element mappings correspondingly. Left: BSE micrograph; Middle top and bottom: Ca and Al mappings; Right top and bottom: Si and Mg mappings.

shown in Fig. 3, magnesium occupies the entire slag grain, with a higher concentration in the core region. In addition, the other elemental mappings in Fig. 7 show that most Ca and Si ions have migrated out, leaving the core enriched in Al and Mg, after full hydration.

Fig. 8(a) reveals EDS linescan-profiles of the elements (Ca, Si, Al, and Mg) along the dissection line A-B in Fig. 7. Mg/Al and Ca/Si atomic ratios, and grey pixel levels on the line are shown in Fig. 8(b) and (c), correspondingly. A clear increase in Mg concentration, while a decrease in Ca and Si concentrations was found in the outer rim. In the adjacent sandwiched zone, the concentration of Mg decreased. Then, the Mg concentration rose towards the core remarkably, even higher than the values measured in the outer rim, leading to a higher Mg/Al ratio in the middle of the dissecting line. As for the grey value, it was about 90 in the outer rim and core, while it increased to approximately 140 in the sandwiched zone.

Based on the results above, it can be postulated that as the hydration progresses in a medium slag grain (of typically 8–17 μm), Mg tends to migrate towards the outer rim and fixed there, leading to a Mg/Al atomic ratio of ~1.5. The newly released Mg^{2+} ions in the core accumulate locally due to their low mobility [6,7,9]. It appears that Al^{3+} ions do also migrate outwards, and a minor increase of Al concentration was observed in the outer rim, in the form of hydrotalcite-like phases together with Mg. On the other hand, due to their high mobility, Ca^{2+} and Si^{4+} ions can readily be dissolved and transported into cement matrix and take part in the formation of C–S–H gel phase [18,22]. The entrapped Ca^{2+} and Si^{4+} ions would play roles in the precipitation of C–S–H gel phase in the sandwiched region.

3.3. Large slag grains

3.3.1. Microstructure

Fig. 9 displays BSE micrographs of two randomly selected microstructure where partially hydrated large (>15 μm) slag particles were observed. These grains can be recognized by their unhydrated core and hydrated thick rim, which are represented with light grey and dark grey pixel colors, respectively. Hydrated rim was developed irregularly surrounding the slag grains and their thickness vary considerably. Preferential development of the rim hydration on one side was also common.

3.3.2. Elemental composition

Fig. 10 illustrates another representative microstructure mainly containing large slag grains, as well as its main element (Ca, Si, Al, and Mg) mappings at a close-up view. No doubt that magnesium is still distributed within the original slag grain boundaries, and most Ca and Si ions dissolved from unreacted slag cores have migrated out, leaving the rims enriched in Al and Mg as a result. However, unlike the observations on the small slag grains (Fig. 3) and medium slag grains (Fig. 7), two cases can be identified for partially hydrated large slag grains. For slag grains indicated as 3-1, the rims are very thin. Al and Mg are accumulated in the rims while Ca and Si migrate out into cement matrix. No clear zonation is observed in this case. For slag grains indicated as 3-2, the rims are apparently thicker. The outer rim rich in Mg appears dark while the Ca and Si concentrations increase in the sandwiched zone (Mg concentration decreases in this zone). When moving inside further, a new region, also abundant in Mg occurs surrounding the unreacted slag cores directly.

Fig. 11 presents EDS linescan-profiles of the elements (Ca, Si, Al, and

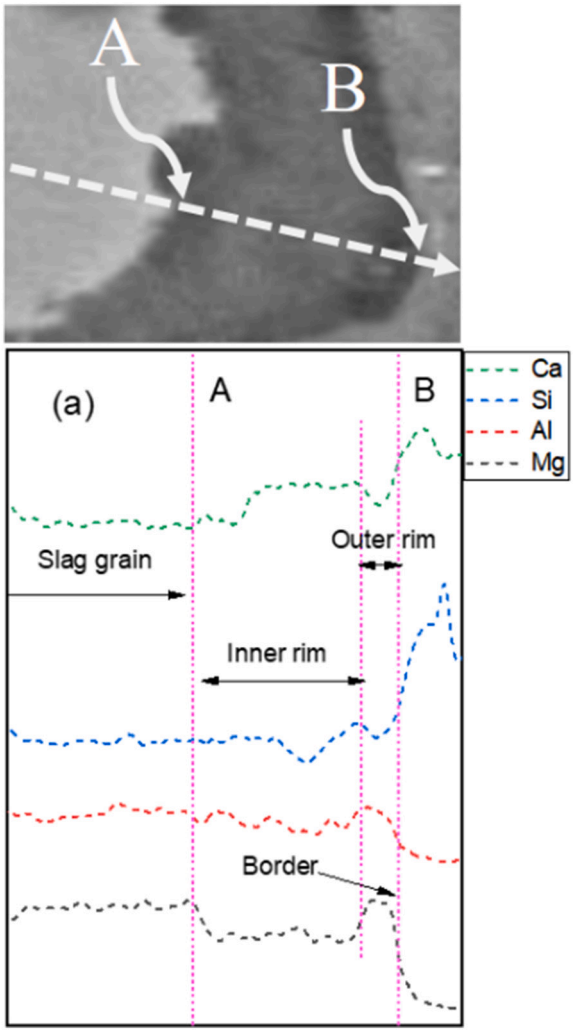

Fig. 11. Linescan-profiles of Ca, Si, Al and Mg along the dissection line A-B (the distance from A to B is <5 μm) shown in Fig. 9(a).

Mg) along the dissection line A-B in Fig. 9(a). The large grain examined here exhibits a commonly observed form of partial hydration, found in early age slag cement pastes. As shown in Fig. 11, a minor increase in Mg content and a decrease in Ca and Si was determined in the outer rim near the grain boundary, while the inner rim showed opposite trend for the concentrations of the same ions.

Fig. 12(a) reveals EDS linescan-profiles of the elements (Ca, Si, Al, and Mg) along the dissection line C-D in Fig. 9(b). Mg/Al and Ca/Si atomic ratios and grey level across the line are shown in Fig. 12(b) and (c), correspondingly. The outer rim rich in Mg appears dark; the sandwiched zone shows a lighter coloration as Ca and Si concentrations increase. As we penetrate further towards the core, a new region, also abundant in Mg occurs which surrounds the unreacted slag core directly.

Mg/Al atomic ratio shown in Fig. 12(b) exhibits a similar trend to that of Mg concentration in Fig. 12(a), which is ~2.0 in the outer rim and the newly formed region, while it decreases to ~1.0 in the sandwiched zone between them. As for the grey value along the line C-D, the value is about 80 on average in the outer rim and newly formed region rich in Al and Mg, while it increases to approximately 120 in the sandwiched zone.

4. A schematic summary and discussion

Fig. 13 shows a typical grey level histogram of the paste component. Three main phases were distinguished by deconvoluting the peaks, namely Hydrotalcite-like phase in the rim of slag, C–S–H gel phase, and anhydrous slag grain.

Phase segmentations were carried out by thresholding grey pixel values (0–255) based on the generated histogram [23]. The range of pixel values of the three segmented phases were 0–100 (blue), 100–160 (origin), and 160–255 (green), which are highlighted with artificial pixel range colorations. Fig. 14 presents one typical micrograph field of view, acquired at 2000× magnification, where the spatial distribution of the three phases is highlighted. In principle, high pixel value (160–255) corresponds to anhydrous slag phases, and minor unhydrated cement clinker. Hydrotalcite-like phase, secondary precipitation from the hydration of slag is represented by low pixel values (0–100). Its distribution was linked to the size of original slag grain significantly. In fully hydrated small slag grains, it accumulates only in the outer rim near the border. In fully hydrated medium slag grains, it occupies the outer rim as well as the core area. Finally in large slag grains the it phases is distributed in the outer rim and within the newly formed region surrounding unreacted slag grains. Pixel values of (100–160) could be assigned to C–S(A)–H gel phase, which is the essential component of cement matrix. Meanwhile, it is also precipitated in the rim of slag. For small slag grain after full hydration, it is formed in the core; as for medium and large slag grain, it exists in the sandwiched zone between two regions rich in hydrotalcite-like phase.

In summary, Fig. 15 gives a schematic summary of the formation and spatial distribution of the hydrates in a fully hydrated slag grain, based on the original size of the parent slag grains. For medium (8–17 μm) and large slag grains (>15 μm), various intermediate (or transition) states are frequently observed even in a well-aged concrete. Each intermediate state appears to act as a precursor for the consequent stage up to the ultimate phase composition. The dissolved Mg ions are fixed into the hydrotalcite-like phase near the grain boundary. At this stage the rim area is composed of two different regions (State 1, 3-1 in Figs. 9 and 10). This configuration is commonly observed in slags with relatively low degree of hydration. As the hydration proceeds, the newly released Mg ions cannot reach the grain boundary and form a new region which was represented as a dark inner ring (State 2, 3-2 in Figs. 9 and 10). With the reaction front proceeding inside, the ultimate distribution of hydrates is assumed to be similar to that of medium slag grain as seen in Fig. 15.

In fact, it becomes increasingly difficult for the continuous dissolution of large slag grain at later age in the actual environment. As confirmed by the TG and XRD results (Fig. 1), portlandite (the source of OH^- ion) has almost been consumed. Furthermore, lack of space for the growth of hydration products may also make the dissolution of large slag grain hard to complete [18].

As mentioned earlier, the hydration of submicron slag grains (<1 μm) is excluded from the scope of this paper. For one thing, it was difficult to observe a clear distribution of hydrates within the original slag grain due to its size. For another, an accurate elemental mapping is not possible due to the minimum electron-solid interaction volume. Nonetheless, according to the observation on small slag grain, it is postulated that after the full hydration of submicron slag grain, Ca and Si move out into the matrix. On the contrary, Mg together with Al takes part in the formation of hydrotalcite-like phase.

It is well recognized that the range of Mg^{2+} ion is restricted within the original slag grain boundary, even for the ions originally positioned near the slag particle surface. At the atomic level, the central Mg^{2+} ion of hydrotalcite-like phase is surrounded by six hydroxyl groups in an octahedral configuration. Through edge-sharing, these octahedral units form infinite, charge-neutral layers, which stack on top of one another to form the three-dimensional structure. The length of interlayer space (d_{003}) is ~1 nm, depending on the exact chemical composition [24–26]. Compared with the size of various ions and molecules, e.g., Ca^{2+}, Si^{4+}, Al^{3+}, OH^-, and H_2O, the interlayer space of hydrotalcite-like phase can be considered as a natural passage for the free transport of these ions and molecules.

When the hydration is initiated at the surface of a slag particle, a high

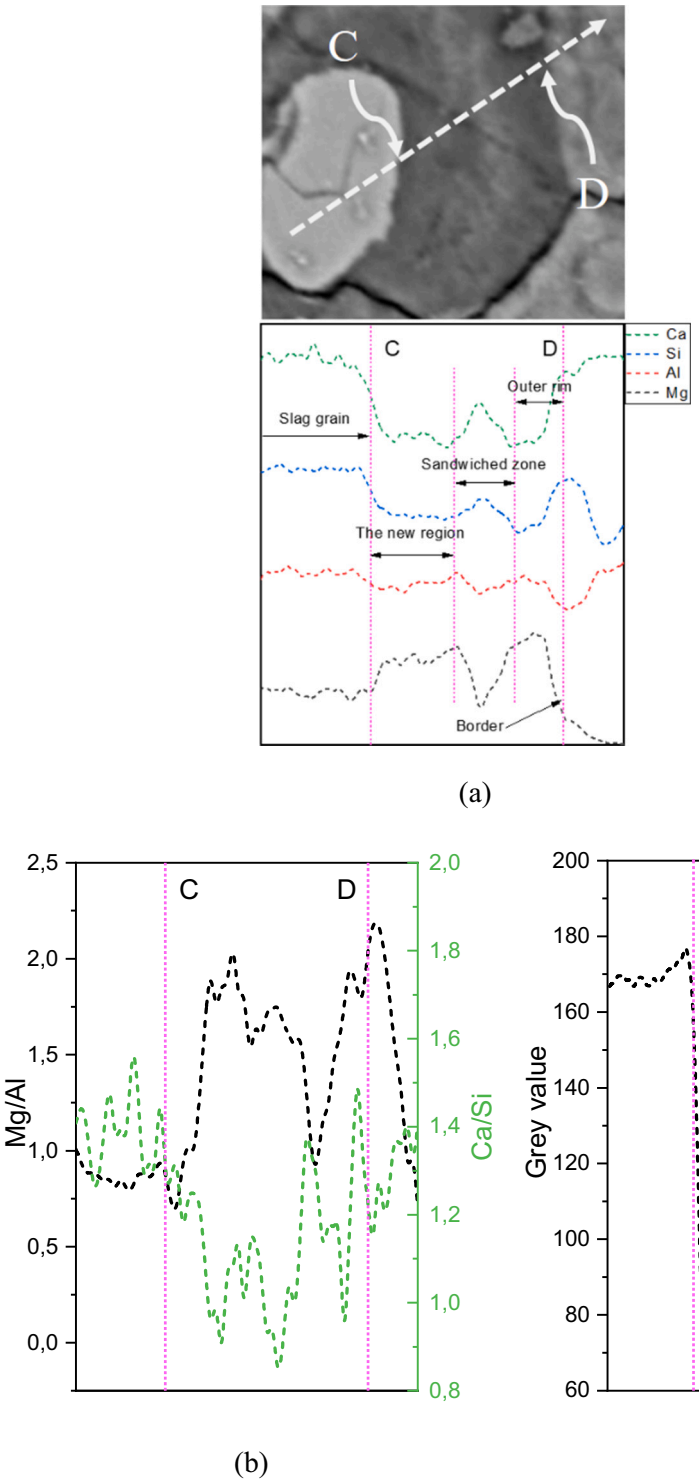

Fig. 12. (a) Linescan-profile of Ca, Si, Al and Mg along the dissection section C-D (the distance from C to D is >5 μm) shown in Fig. 9(b); (b) Mg/Al and Ca/Si atomic ratios and (c) grey level correspondingly.

supersaturation, inducing high nucleation rate leads to the precipitation of nano-sized (amorphous or microcrystalline) hydrotalcite-like phase. They are distributed homogenously at this stage [22], as shown in Fig. 15. With the reaction advancing progressively, amorphous, or microcrystalline hydrotalcite-like phase would undergo the onset of Lifshitz-Slyozov instability [27], and larger, more stable hydrotalcite-like phase crystals grow at the expense of the smaller ones. A band or ring is formed where these large and stable crystals are concentrated, i.e., zone which was defined as the outer rim in this study. This process is also known as Ostwald ripening [28]. For a small slag particle, even the newly released magnesium (in the form of nanometer-sized hydrotalcite-like phase) from the core could migrate to the grain boundary after a long hydration time (The radius of a small slag particle is <4 μm.). For Ca^{2+}, Si^{4+}, and Al^{3+} ions dissolved from the core area, due to their fair mobility, they can also diffuse (concentration difference, diffusion-type) outside into the matrix, passing through the interlayer space of hydrotalcite-like phase formed in the outer rim. The ion concentration equilibrium between cement matrix and the core of slag was

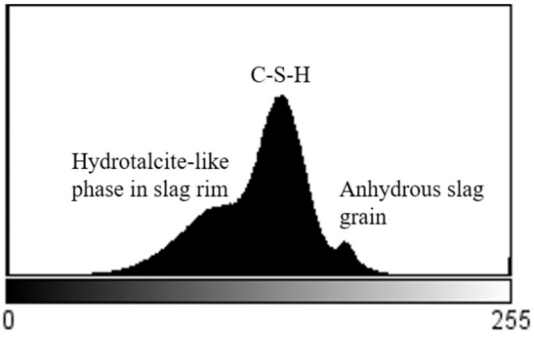

Fig. 13. A typical grey level histogram of the paste component in the concrete sample.

further confirmed by the same grey-scale coloration between them.

The larger the size of a slag grain, the harder it is for the newly released magnesium ions to reach the outer rim due to their low mobility [22], thus, it accumulates locally to form an additional hydrotalcite-like region in the core of a medium slag grain or render a hydrotalcite-like region that is connected to the unreacted slag core of a large slag grain. In Part 3.3, it is shown that when the rim is thick enough (>5 μm), Mg accumulates locally. In other words, the maximum migration distance of magnesium is around ~4 μm, and it also explains that for a small slag grain, even the magnesium in the innermost could move to the boundary, leaving the core without any trace of it.

Our findings suggest that it is the size of a slag grain and the low mobility of magnesium that determine the ultimate form and spatial distribution of the hydrates in the slag rim. Considering these hydration product characteristics would improve the accuracy of the slag hydration simulations as none of the existing models relate the original slag size to the generated phase zoning within the slag grain. Furthermore, it should be emphasized that hydrotalcite-like phases occupy a net positive volume upon full hydration in a medium or large slag grain. Greater accumulation of hydrotalcite-like phase in the slag rim could increase the durability of slag cement paste, as it has strong capacity to fix chloride (Cl^-) [29–31], sulfate (SO_4^{2-}) [32,33], carbonate (CO_3^{2-}) [34–36], and other potentially harmful species, as interlayer ions. However, because the larger a slag grain, the slower it hydrates, a medium-sized slag grain appears to be a good compromise between slag hydration degree and the amount of hydrotalcite-like phase produced. Based on the results of our investigation, we believe that there is great interest in studying the effects of increased 5–15 μm grain (corresponding to medium-sized slag grain roughly in this paper) fraction on

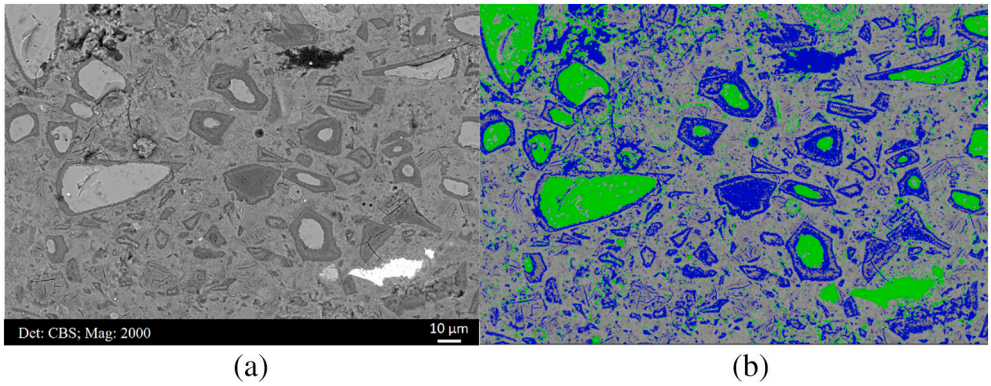

Fig. 14. (a): One typical micrograph of the microstructure; (b): distribution of three groups of grey value or three phases, i.e., 0–100 (blue, hydrotalcite-like phase in slag rim), 100–160 (origin, C–S–H gel phase), and 160–255 (green, anhydrous slag grain). (For interpretation of the references to color in this figure legend, the reader is referred to the web version of this article.)

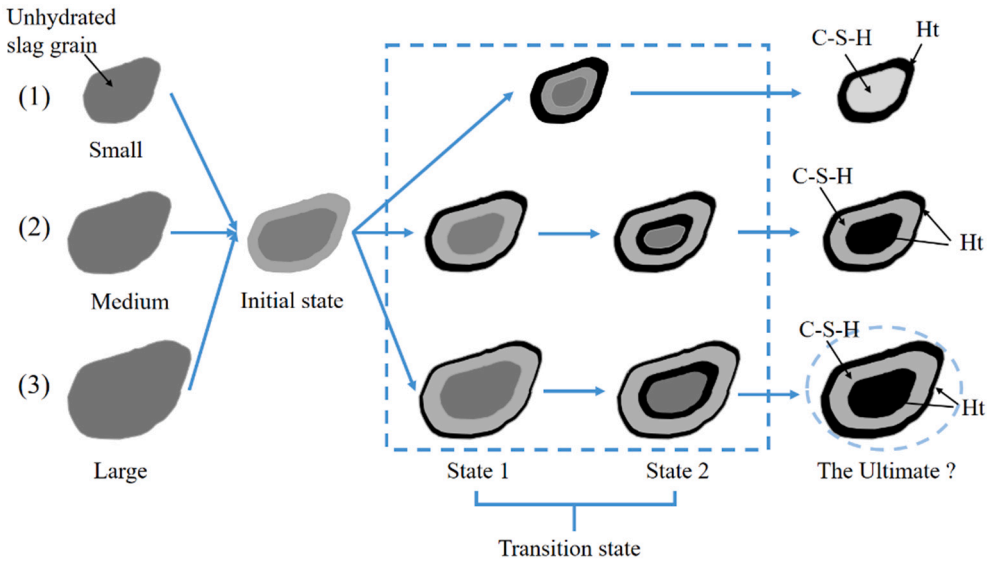

Fig. 15. A schematic illustration about the formation and spatial distribution of hydrates of slag grain with different original sizes after full hydration. Ht: hydrotalcite-like phase.

the hydration and durability characteristics of slag cement which could potentially open new service life design opportunities for slag-rich cement concrete. One the other hand, one should keep in mind that the increased medium-sized fraction would decrease the early age compressive strength, etc. of the blended system, as these early age properties depend on the hydration of small slag grains significantly.

5. Conclusions

The paper characterized the elemental composition of hydrates distributed in the slag rims of a 40-year-old slag cement concrete collected from the field. The form and distribution of the hydrates resulting from the full hydration of slag grains were identified and classified based on the slag size. Overall, it is the size of slag grain and the low mobility of magnesium that determine the ultimate form and spatial distribution of hydrates in the rim. The main conclusions were drawn as follows:

- For a small slag grain (<8 μm) upon full hydration, two distinct regions corresponding to entirely different hydrates are formed. The outer rim is rich in aluminum and magnesium, leading to the precipitation of hydrotalcite-like phase. Calcium and silicon entrapped in the core lead to the formation of C–S–H gel phase.
- As for the medium slag grains (8–17 μm), three regions are clearly visible after full hydration. Hydrotalcite-like phase is mainly formed in the outer rim and core. C–S–H gel phase precipitates between the inner and the outer hydrotalcite-like rings.
- Different intermediates (or transition states) exist during the hydration of large slag grains (>15 μm). Upon dissolution, Mg ions are captured and fixed at the outer rim. As the hydration proceeds, the newly released Mg ions cannot migrate far away. They are deposited around the unhydrated slag region to form a new local hydrotalcite-like rich region.
- Medium-sized slag grain seems to be a good compromise between slag hydration degree and the amount of hydrotalcite-like phase produced. Our findings suggest that there is great potential in increasing the medium-sized slag grain fraction during cement manufacturing for an enhanced durability-related performance in slag-rich cement concrete.

CRediT authorship contribution statement

Yu Zhang: Investigation, Methodology, Experiment, Analysis, Writing - Original draft preparation, Writing - Review & editing. Oğuzhan Çopuroğlu: Supervision, Funding acquisition, Review & editing.

Declaration of competing interest

The authors declare no conflict of interest.

Data availability

Data will be made available on request.

Acknowledgements

China Scholarship Council (the grant number 201808320456) and BAM Infraconsult B.V. are gratefully acknowledged for their financial support. Authors thank Arjan Thijssen (Microlab, TU Delft) for his technical support. Bart Hendrix (Microlab, TU Delft) shared the samples from the field for investigation, and authors would also like to thank him.

Appendix A. Supplementary data

Supplementary data to this article can be found online at https://doi.org/10.1016/j.cemconres.2022.106985.

References

[1] J. Bijen, Benefits of slag and fly ash, Constr. Build. Mater. 10 (5) (1996) 309–314.
[2] M. Juenger, et al., Advances in alternative cementitious binders, Cem. Concr. Res. 41 (12) (2011) 1232–1243.
[3] E. Crossin, The greenhouse gas implications of using ground granulated blast furnace slag as a cement substitute, J. Clean. Prod. 95 (2015) 101–108.
[4] Y. Li, et al., Environmental impact analysis of blast furnace slag applied to ordinary Portland cement production, J. Clean. Prod. 120 (2016) 221–230.
[5] W. Chen, H. Brouwers, The hydration of slag, part 2: reaction models for blended cement, J. Mater. Sci. 42 (2) (2007) 444–464.
[6] J.-I. Escalante-Garcia, J. Sharp, The chemical composition and microstructure of hydration products in blended cements, Cem. Concr. Compos. 26 (8) (2004) 967–976.
[7] K. Luke, E. Lachowski, Internal composition of 20-year-old fly ash and slag-blended ordinary Portland cement pastes, J. Am. Ceram. Soc. 91 (12) (2008) 4084–4092.
[8] J. Escalante, et al., Reactivity of blast-furnace slag in Portland cement blends hydrated under different conditions, Cem. Concr. Res. 31 (10) (2001) 1403–1409.
[9] R. Taylor, I. Richardson, R. Brydson, Composition and microstructure of 20-year-old ordinary Portland cement–ground granulated blast-furnace slag blends containing 0 to 100% slag, Cem. Concr. Res. 40 (7) (2010) 971–983.
[10] V. Kocaba, Development And Evaluation of Methods to Follow Microstructural Development of Cementitious Systems Including Slags, EPFL, 2009.
[11] I. Richardson, G. Groves, The structure of the calcium silicate hydrate phases present in hardened pastes of white Portland cement/blast-furnace slag blends, J. Mater. Sci. 32 (18) (1997) 4793–4802.
[12] I.G. Richardson, The nature of CSH in hardened cements, Cem. Concr. Res. 29 (8) (1999) 1131–1147.
[13] B. Langan, K. Weng, M. Ward, Effect of silica fume and fly ash on heat of hydration of Portland cement, Cem. Concr. Res. 32 (7) (2002) 1045–1051.
[14] M. Meyn, K. Beneke, G. Lagaly, Anion-exchange reactions of layered double hydroxides, Inorg. Chem. 29 (26) (1990) 5201–5207.
[15] H.F. Taylor, Cement Chemistry Vol. 2, Thomas Telford, London, 1997.
[16] X. Ke, S.A. Bernal, J.L. Provis, Uptake of chloride and carbonate by Mg-Al and Ca-Al layered double hydroxides in simulated pore solutions of alkali-activated slag cement, Cem. Concr. Res. 100 (2017) 1–13.
[17] I. Richardson, S. Li, Composition and structure of an 18-year-old 5M KOH-activated ground granulated blast-furnace slag paste, Constr. Build. Mater. 168 (2018) 404–411.
[18] B. Li, Q. Li, W. Chen, Spatial zonation of a hydrotalcite-like phase in the inner product of slag: new insights into the hydration mechanism, Cem. Concr. Res. 145 (2021), 106460.
[19] Z. Jia, et al., The characteristics and formation mechanism of the dark rim in alkali-activated slag, Cem. Concr. Compos. 112 (2020), 103682.
[20] H. Ye, Nanoscale attraction between calcium-aluminosilicate-hydrate and Mg-Al layered double hydroxides in alkali-activated slag, Mater. Charact. 140 (2018) 95–102.
[21] Yu Zhang, S. Karthikeyan, Ç. Oğuzhan, EDS microanalysis of unhydrated blast furnace slag grains in field concrete with different service life, Microsc. Microanal. (2022) 1–11.
[22] Q. Feng, E. Lachowski, F. Glasser, Densification and migration of ions in blast furnace slag-Portland cement pastes, MRS Online Proc.Library Arch. 136 (1988).
[23] V. Kocaba, E. Gallucci, K.L. Scrivener, Methods for determination of degree of reaction of slag in blended cement pastes, Cem. Concr. Res. 42 (3) (2012) 511–525.
[24] S. Miyata, Physico-chemical properties of synthetic hydrotalcites in relation to composition, Clay Clay Miner. 28 (1) (1980) 50–56.
[25] S. Miyata, Anion-exchange properties of hydrotalcite-like compounds, Clay Clay Miner. 31 (4) (1983) 305–311.
[26] W.T. Reichle, Synthesis of anionic clay minerals (mixed metal hydroxides, hydrotalcite), Solid State Ionics 22 (1) (1986) 135–141.
[27] I.M. Lifshitz, V.V. Slyozov, The kinetics of precipitation from supersaturated solid solutions, J.Phys.Chem.Solids 19 (1–2) (1961) 35–50.
[28] W. Dunning, Ripening And Ageing Processes in Precipitates, 1973.
[29] J. Csizmadia, G. Balázs, F.D. Tamás, Chloride ion binding capacity of aluminoferrites, Cem. Concr. Res. 31 (4) (2001) 577–588.
[30] Z. Yang, H. Fischer, R. Polder, Synthesis and characterization of modified hydrotalcites and their ion exchange characteristics in chloride-rich simulated concrete pore solution, Cem. Concr. Compos. 47 (2014) 87–93.
[31] M. Balonis, et al., Impact of chloride on the mineralogy of hydrated Portland cement systems, Cem. Concr. Res. 40 (7) (2010) 1009–1022.
[32] L. Guo, et al., Improving sulfate attack resistance of concrete by using calcined Mg-Al-CO3 LDHs: adsorption behavior and mechanism, Constr. Build. Mater. 232 (2020), 117256.
[33] J. Xu, Q. Tan, Y. Mei, Corrosion protection of steel by Mg-Al layered double hydroxides in simulated concrete pore solution: effect of SO42, Corros. Sci. 163 (2020), 108223.

[34] S. Walspurger, et al., High CO2 storage capacity in alkali-promoted hydrotalcite-based material. In situ detection of reversible formation of magnesium carbonate, Chem. Eur. J. 16 (42) (2010) 12694–12700.
[35] P. Duan, et al., Influence of layered double hydroxides on microstructure and carbonation resistance of sulphoaluminate cement concrete, Constr. Build. Mater. 48 (2013) 601–609.
[36] Z. Shui, et al., Improvement of concrete carbonation resistance based on a structure modified layered double hydroxides (LDHs): experiments and mechanism analysis, Constr. Build. Mater. 176 (2018) 228–240.